Comparison of image quality with ^{62}Cu and ^{64}Cu-labeled radiotracers in positron emission tomography whole-body phantom imaging

Masato Kobayashi[1] PhD,
Tetsuya Mori[2] PhD,
Tetsuya Tsujikawa[2] MD, PhD,
Kazuhiro Ogai[1] PhD,
Jyunko Sugama[1] PhD,
Yasushi Kiyono[2] PhD,
Keiichi Kawai[2,3] PhD,
Hidehiko Okazawa[2] MD, PhD

1. Wellness Promotion Science Center, Institute of Medical, Pharmaceutical and Health Sciences, Kanazawa University, Kanazawa, Japan
2. Biomedical Imaging Research Center, University of Fukui, Fukui, Japan
3. School of Health Sciences, College of Medical, Pharmaceutical and Health Sciences, Kanazawa University, Kanazawa, Japan

Keywords: ^{64}Cu - Acquisition mode
-Reconstruction algorithm
-Image quality - ^{62}Cu radiotracers

Correspondence address:
Masato Kobayashi PhD,
Wellness Promotion Science Center Institute of Medical,
Pharmaceutical and Health Science, Kanazawa University
5-11-80 Kodatsuno,
Kanazawa 920-0942, Japan
Tel: +81-76-265-2500;
Fax: +81-76-234-4366
kobayasi@mhs.mp.kanazawa-u.ac.jp

Received:
22 April, 2015
Accepted revised:
20 May, 2015

Abstract

Objective: PET imaging is possible with copper (Cu) isotopes, ^{60}Cu, ^{61}Cu, ^{62}Cu and ^{64}Cu. Although ^{62}Cu- and ^{64}Cu-labeled radiotracers are often used for preclinical and clinical PET studies, we do not know which radiotracers have better image quality for tumor imaging. In this study, we compare image quality between ^{62}Cu and ^{64}Cu imaging with a different acquisition mode and reconstruction algorithm using a whole-body phantom for tumor imaging. **Methods**: In a National Electrical Manufacturers Association (NEMA) 2001 whole-body phantom, the concentration of ^{62}Cu-ATSM and ^{64}Cu-ATSM was, respectively, approximately 2.7 and 1.8MBq/mL in all the spheres and approximately 0.9 and 0.6MBq/mL in the background. After adjustment for true coincidence events between ^{62}Cu and ^{64}Cu, two-dimensional (2D) and three-dimensional (3D) PET scan data were acquired for 10min. The data were reconstructed using filtered back projection (FBP) and the ordered subset expectation maximization (OSEM) algorithm. Image quality of ^{62}Cu and ^{64}Cu was compared using recovery coefficient (RC), sphere-to-background ratio (SBR) and coefficient of variation (%COV). **Results**: There were little significant differences between ^{62}Cu and ^{64}Cu imaging, visually. Recovery coefficients of ^{64}Cu images were higher than those of ^{62}Cu images. The RC of ^{64}Cu images with 3D acquisition mode and OSEM was the highest in all experiments. No SBR values were significantly different from the true value of 3.0 in 37mm sphere diameters, but 3D acquisition and OSEMyielded slight overestimations compared with 2D acquisition and FBP, the gold standard for quantification in PET studies. Percentage COV values of ^{64}Cu with OSEM were significantly lower than those of ^{62}Cu. **Conclusions**: Copper-64 radiotracers provide higher image quality than ^{62}Cu-radiotracers in whole-body tumor imaging only when the 3D acquisition mode and OSEM algorithm are applied. However, the quantitative values for smaller tumors may be slightly overestimated.

Hell J Nucl Med 2015; 18(2): 103-107 *Epub ahead of print: 19 July 2015* *Published online: 5 August 2015*

Introduction

Copper (Cu)-labeled radiotracers have been used in some basic science research and for clinical PET. In particular, Cu-pyruvaldehyde-bis(N4-methylthiosemicarbazone) (Cu-PTSM) [1] and Cu-diacetyl-bis(N4-methylthiosemicarbazone) (Cu-ATSM) [2] have been applied as potential markers of hypoxia and perfusion, respectively. Most clinical Cu-PTSM/ATSM studies have used the short-lived positron-emitting radionuclide of ^{60}Cu [3] or ^{62}Cu [4-7] (Table 1). Copper-64 is potentially useful for not only tumor imaging [8] but also tumor therapeutics [9]. In these radiotracers, the amount of annihilation γ- rays following to β+-decay yields higher image quality in Cu PET imaging unless saturation of the detector occurs. Lewis et al. (2008) reported ^{64}Cu-ATSM appeared to have a higher image quality than ^{60}Cu-ATSM in cancer of the uterine cervix [10]. However, the high-energy positron and gamma emissions of ^{60}Cu, compared to ^{64}Cu, are the greatest disadvantages of using ^{60}Cu as a PET imaging agent[10]. In addition, they did not consider that true coincidence events between ^{60}Cu- and ^{64}Cu-ATSM imaging should be adjusted, although the radiation doses of the two radiotracers were the similar in whole body imaging.

Instead of ^{60}Cu, ^{62}Cu-ATSM has been utilized because ^{62}Cu-ATSM generates ^{62}Zn/^{62}Cu [11-13] and it is less expensive. Moreover, a clinical study showed that the radiation exposure from ^{62}Cu is lower than that from ^{60}Cu [14].

However, we do not know which radiotracers of ^{62}Cu and ^{64}Cu have better image quality for tumor imaging. In this study, we compare image quality between ^{62}Cu and ^{64}Cu imaging with different acquisition modes and reconstruction algorithms using a National Electrical Manufacturers Association (NEMA) 2001 whole-body phantom.

Materials and methods

Preparation of ^{62}Cu- and ^{64}Cu-ATSM

The ^{62}Cu-glycine (no-carrier-added ^{62}Cu) solution was obtained from a ^{62}Zn/^{62}Cu generator system [15]. Copper-62 - ATSM was prepared with a simple mixture of ^{62}Cu solution (5mL) and 0.2mL of ATSM solution (0.5mM in dimethyl sulfoxide) in a sterilized vial [2, 16]. The radiochemical purity of ^{62}Cu-ATSM was confirmed with high-performance liquid chromatography using authentic unlabeled Cu-ATSM before the phantom study. The radiochemical purity of ^{62}Cu-ATSM was greater than 95%.

^{64}Cu was produced as reported previously [17]. The purification of ^{64}Cu and the preparation of ^{64}Cu-ATSM were performed according to previously reported procedures [17, 18]. The radiochemical purity of the resulting ^{64}Cu-ATSM was greater than 95%, as assessed by silica gel thin-layer chromatography (TLC; silica gel 60; Merck, Whitehouse Station, NJ, USA) with ethyl acetate as the mobile phase [19]. Radioactivity levels on the TLC plates were analyzed with a bioimaging analyzer (FLA-7000; Fujifilm, Tokyo, Japan). Elemental $^{62/64}$Cu could not be used for this phantom study because the $^{62/64}$Cu attached to the sidewalls of the whole-body phantom. Consequently, we have used $^{62/64}$Cu-ATSM, a type of ^{62}Cu or ^{64}Cu-labeled radiotracer.

Phantoms

A NEMA 2001 whole-body phantom [20], an elliptical phantom with six individually fillable spheres whose diameters are 10, 13, 17, 22, 28, and 37mm, was prepared. The concentration of ^{64}Cu-ATSM in all spheres was approximately 1.8MBq/mL, which is as dense as that seen in a tumor in a clinical scan [10]. The background was approximately 0.6MBq/mL for ^{64}Cu-ATSM. However, the concentration of ^{62}Cu-ATSM was approximately 2.7MBq/mL in all spheres, with a background of approximately 0.9MBq/mL because we prepared the phantoms to have the same radioactive counts between ^{62}Cu and ^{64}Cu, considering the half-life of ^{62}Cu (23.7min) and ^{64}Cu (12.7h) because their image quality can be compared when their radioactive counts are almost the same. Before starting the acquisition, we regulated and adjusted the true coincidence counts between ^{62}Cu-ATSM and ^{64}Cu-ATSM.

PET scan

The study was approved by the Ethics Committee of the University of Fukui, Faculty of Medical Sciences. A whole-body PET scanner (Advance; GE Healthcare, Milwaukee, Wisconsin, USA) capable of simultaneous acquisition of 35 image slices, with an interslice spacing of 4.25mm, was used for data acquisition [21]. This scanner has 12,096 bismuth germanate crystals with transaxial, axial and radial dimensions of 4.0, 8.1 and 30mm, respectively. The phantom was positioned at the center in the scanner. Two-dimensional (2D) and three-dimensional (3D) dynamic PET scans with 1 frame/min were acquired for 10 min. A 10-min post-injection transmission scan was acquired after the emission scan with a ^{68}Ge/^{68}Ga rod source for attenuation correction.

Reconstruction

The data were reconstructed using a filtered back projection (FBP) algorithm with 0.4 cycle/pixel Hanning filter. For 2D PET, an ordered subset expectation maximization (OSEM) algorithm was applied using four iterations and 28 subsets, a 128×128 matrix, and post-smoothing with a 2.8mm full-width at half maximum (FWHM) post-filter. The 3D data were converted into sets of contiguous transaxial 2D sinograms using Fourier rebinning (FORE). Images 3D were reconstructed using FORE with FBP and FORE with OSEM followed by a weighted least-squares algorithm using three iterations and 32 subsets. 3D Gaussian post-smoothing was applied using 2mm FWHM. The parameters used for the reconstruction algorithms of both 2D and 3D datasets have been optimized in previous studies [22, 23] and by matching of noise on background areas between 2D and 3D images. The scatter correction method was used with the convolution subtraction method [24, 25]. In addition, normalize correction, delayed coincidence correction, dead time correction, and decayed correction were incorporated in the reconstruction algorithm. After reconstruction, the data was used to generate summed images of 10min from dynamic data of 1 frame/min.

Image analysis

Circular volumes of interest (VOI) were placed over visible and invisible hot sphere locations on the images using the corresponding transmission images. VOI (10cm) were also located in the background area.

The recovery coefficient (RC) was calculated using the following formula:

RC (%)=A/B×100,where A is the mean pixel counts of each hot sphere, and B is the known radioactive counts obtained using the gamma counter. Image noise of RC was defined as the coefficient of variation (%COV), standard deviation / mean×100 %) of pixel values within the VOI on sphere diameter areas and background areas.

The sphere-to-background ratio (SBR) of approximately 3:1 was regulated corresponding to an injected patient activity of 370MBq(10mCi) of ^{62}Cu-ATSM, assuming a typical patient weight of 70kg [5-7]. SBRs were calculated using mean pixel counts of each diameter sphere divided by those of background.

Statistical analysis

A statistical software package (JMP® version 9 SAS Institute Inc., Cary, NC, USA) was used for statistical analysis. We applied a Wilcoxon test for comparison of ^{62}Cu and ^{64}Cu or analysis of RC, SBR and %COV for 2D and 3D acquisition mode with FBP and OSEM algorithms, which were used as a multiplex analysis with a population mean value. Statistically significant differences were defined as $P< 0.05$.

Results

Figure 1 shows images of the whole-body phantom. There were little significant differences between ^{62}Cu and ^{64}Cu imaging, visually. We could not identify the smallest sphere region (10mm diameter) in all cases.

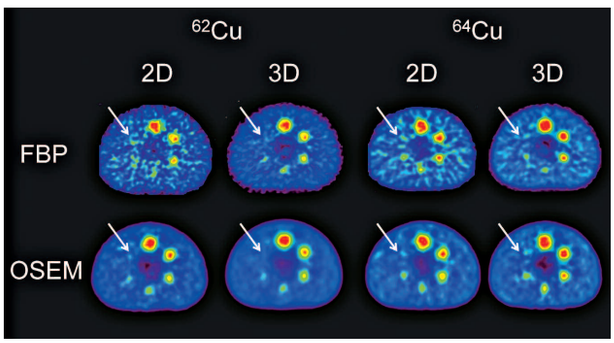

Figure 1. Images of the whole-body phantom at a ratio of sphere activity to background activity of 3.0.

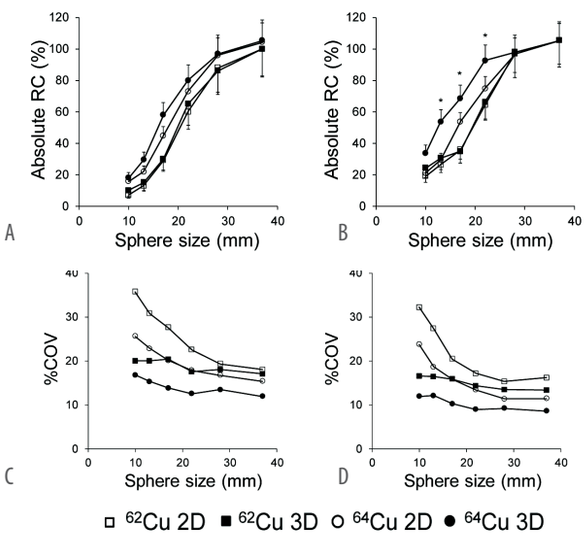

Figure 2. RC and %COV with 2D and 3D acquisition mode and FBP (A, C) and OSEM (B, D) algorithms. RCs of ^{64}Cu images were higher than those of ^{62}Cu images. 3D acquisition and OSEM algorithm provided the highest RC on ^{64}Cu images. %COV of ^{64}Cu images were lower than those of ^{62}Cu images. 3D acquisition yielded lower percentCOV than 2D acquisition, and OSEM reduced %COV compared with FBP. * P< 0.05 vs. ^{64}Cu images with 2D acquisition mode for RC.

We could not identify the smallest sphere region (10mm diameter, arrow) with either the FBP or OSEM algorithm. There were no significant differences between ^{62}Cu and ^{64}Cu imaging, visually.

In Figure 2, RCs of ^{64}Cu images were higher than those of ^{62}Cu images. Especially, 3D acquisition and OSEM produced the highest RC on ^{64}Cu images. percent COV of ^{64}Cu images were lower than those of ^{62}Cu images. 3D acquisition yielded lower %COV than 2D acquisition, and OSEM reduced percent COV compared with FBP.

No SBR values were significantly different from the true value of 3.0 in 37mm sphere diameters (Table 2). In ^{64}Cu imaging, 3D acquisition and OSEM significantly elevated SBR in comparison with 2D acquisition and FBP in 13, 17 and 22mm sphere diameters. In background areas, %COV values of ^{64}Cu with OSEM were significantly lower than those of ^{62}Cu with OSEM (Table 3).

Discussion

PET imaging of ^{64}Cu had higher image quality than that of ^{62}Cu in the whole-body phantom only when the 3D acquisition mode and OSEM algorithm were applied, although these differences were little apparent visually in the phantom images. RCs of ^{64}Cu images were also greater than those of ^{62}Cu images (Fig. 2a, b) because ^{62}Cu has a higher maximum energy of β+ (Table 1), and consequently has a longer positron range than ^{64}Cu [26]. The 3D acquisition mode and OSEM algorithm yielded the highest RC on ^{64}Cu images. Fakhri et al. (2007) reported that 3D acquisition produced greater image quality in normal-sized patients [27]. Lartizien et al. (2004) also reported that the full 3D mode and Fourier rebinning OSEM offered better or equivalent detection performance than the 2D mode and OSEM for the same injected dose typically used in clinical practice [28]. As shown in Fi-

***Table 1**. Decay properties of Cu radioisotopes.*

Isotope	Half-life	β^- (MeV)	β^+(MeV)	β^+ intensity (%)	EC (%)	γ (MeV)	γ intensity (%)
^{60}Cu	23.7min	-	1.91 1.98 2.95 3.77 (2.94)	11.6 49 15 5	7.2	0.511 0.826 1.33 1.79 3.12	185 21.7 88 45.4 4.8
^{61}Cu	3.3h	-	0.93 1.22 (1.16)	5.5 51	36	0.283 0.373 0.511 0.656 1.19	12.2 2.1 123 10.8 3.7
^{62}Cu	9.67min	-	2.93	97.2	2	0.511 0.511	195 35.2
^{64}Cu	12.7h	0.579	0.65	17.6	40	1.35	0.5

β^-: electron; β^+: positron; EC: electron capture; γ: gamma emission; ( ): average of end-point-energies

Table 2. *Average SBR values with 2D and 3D acquisition mode and FBP and OSEM algorithms without RC in all sphere sizes.*

Isotope	^{62}Cu				^{64}Cu			
Acquisition mode	2D		3D		2D		3D	
Sphere size (mm)	FBP	OSEM	FBP	OSEM	FBP	OSEM	FBP	OSE
10	0.95	0.97	0.95	0.97	0.97	0.97	0.96	1.01
13	1.39	1.40	1.41	1.40	1.46	1.51[b]	1.48	1.61[a]
17	1.87	1.88	1.90	1.88	1.84	1.90[b]	1.89	1.99[a]
22	2.03	2.05	2.05	2.05	2.05	2.07	2.06	2.11[b]
28	2.84	2.85	2.86	2.85	2.84	2.86	2.86	2.87
37	3.00	3.05	3.02	3.05	3.03	3.04	3.05	3.06

2D: two-dimensional scan; 3D: three-dimensional scan; FBP: filtered back projection; OSEM: ordered subset expectation maximization; a[P]< 0.01 and b[P]< 0.05 vs. 2D acquisition and FBP of ^{62}Cu or ^{64}Cu.

Table 3. *Average % COV with 2D and 3D acquisition mode and FBP and OSEM algorithms on background areas.*

	2D		3D	
	FBP	OSEM	FBP	OSEM
^{62}Cu	19.7	15.1	18.9	14.4
^{64}Cu	18.4	13.7[a]	17.5	11.3[a]

2D: two-dimensional scan; 3D: three-dimensional scan; FBP: filtered back projection; OSEM: ordered subset expectation maximization; [a]P< 0.05 vs. ^{62}Cu.

gure 2 and Table 3, 3D acquisition decreased image noise compared with 2D acquisition. Lodge et al. (2006) reported that 3D PET acquisition reduced image noise on 2-[^{18}F]fluoro-2-deoxy-D-glucose (^{18}F-FDG) PET [29]. In addition, OSEM decreased the noise compared with FBP (Figure 2c, d). Therefore, we estimate a combination of 3D acquisition mode and OSEM algorithm produces better RC and %COV for tumor imaging with Cu radioisotopes.

SBR values were not different from the true value of approximately 3.0 in 37mm sphere diameters (Table 2). 2D acquisition and OSEM showed similar SBR values with 2D acquisition and FBP, the gold standard for quantification in PET studies using both Cu isotopes. Chen et al. (2007) also reported that the quantification of $^{13}NH_3$ PET using 2D acquisition and OSEM was similar to that using 2D acquisition and FBP [30]. Our results show that ^{64}Cu imaging with OSEM gave slight overestimations compared with FBP because OSEM reduced the positive bias from the non-negativity constraint and the inaccuracy of Poisson statistics, (Table 2). Despite the overestimation, the combination of 3D acquisition and OSEM provides better image quality for whole-body tumor imaging with both Cu radiotracers. %COV values of ^{64}Cu with OSEM were significantly lower than those of ^{62}Cu (Table 3). Especially, 3D acquisition and OSEM significantly yielded the lowest %COV in all cases because the combination had the lowest standard deviation.

Although the shorter half-lives and higher positron decay fractions of ^{60}Cu and ^{62}Cu make them suitable for characterizing the faster kinetics of blood flow, etc., the higher sensitivity of ^{60}Cu and ^{62}Cu has been used for slower kinetic tumor imaging because ^{61}Cu and ^{64}Cu need enriched targets and increase overall costs [31, 32]. The longer half-lives of ^{61}Cu and ^{64}Cu are basically better suited to studying tumor imaging; however, they result in higher radiation doses. In particular, ^{64}Cu provides the highest radiation doses to humans among the Cu radioisotopes [14]. Although each Curadioisotope has unique advantages and disadvantages for tumor imaging, in previous literature on image quality, ^{64}Cu-ATSM had higher image quality than ^{60}Cu-ATSM in cancer of the uterine cervix [10]. We surmise that ^{62}Cu-ATSM can produce a better image quality than ^{60}Cu-ATSM because ^{60}Cu exhibits high radioactivity from γ rays compared with ^{62}Cu, which emits just single γ rays (0.511MeV). With ^{62}Cu imaging, it may be possible to acquire emission data for up to 30min because of the shorter half-life; however, ^{62}Cu images acquired over 10min will be similar to those acquired over 30min and can be compared with ^{64}Cu images acquired over 10min. Therefore, including our results, ^{64}Cu imaging produces the highest image quality in clinical Cu PET imaging when the 3D acquisition mode and OSEM algorithm are applied. However, specific Cu radioisotopes may need to be selected for each examination because of the potential radiation dose to patients. We must also be wary of potentially overestimated results when combining 3D acquisition and the OSEM algorithm in Cu imaging.

In conclusion, ^{64}Cu radiotracers provide higher image quality than ^{62}Cu radiotracers in whole-body tumor imaging. Although ^{64}Cu imaging has better image quality when using a combination of a 3D acquisition mode and OSEM algorithm, the quantitative values for small tumors may be slightly overestimated.

Acknowledgements

The author thanks the staff members at the Biological Imaging Research Center, University of Fukui for their technical support.

The authors declare that they have no conflicts of interest.

Bibliography

1. Green MA, Klippenstein DL, Tennison JR. Copper(II) bis(thiosemicarbazone) complexes as potential tracers for evaluation of cerebral and myocardial blood flow with PET. *J Nucl Med* 1988; 29: 1549-57.
2. Fujibayashi Y, Taniuchi H, Yonekura Y et al. Copper-62-ATSM: a new hypoxia imaging agent with high membrane permeability and low redox potential. *J Nucl Med* 1997; 38: 1155-60.
3. Dehdashti F, Mintun MA, Lewis JS, et al.In vivo assessment of tumor hypoxia in lung cancer with ^{60}Cu-ATSM. *Eur J Nucl Med Mol Imaging* 2003; 30: 844-50.
4. Okazawa H, Yonekura Y, Fujibayashi Y et al. Clinical application and quantitative evaluation of generator-produced copper-62-PTSM as a

brain perfusion tracer for PET. *J Nucl Med* 1994; 35: 1910-15.
5. Wong TZ, Lacy JL, Petry NA et al. PET of hypoxia and perfusion with ^{62}Cu-ATSM and ^{62}Cu-PTSM using a ^{62}Zn/^{62}Cu generator. *Am J Roentgenol* 2008; 190: 427-32.
6. Lohith TG, Kudo T, Demura Y et al. Pathophysiologic correlation between ^{62}Cu-ATSM and ^{18}F-FDG in lung cancer. *J Nucl Med* 2009; 50: 1948-53.
7. Kositwattanarerk A, Oh M, Kudo T et al. Different distribution of ^{62}Cu-ATSM and ^{18}F-FDG in head and neck cancers. *Clin Nucl Med* 2012; 37: 252-7.
8. Lewis JS, McCarthy DW, McCarthy TJ et al. Evaluation of ^{64}Cu-ATSM in vitro and in vivo in a hypoxic tumor model. *J Nucl Med* 1999; 40: 177-83.
9. Lewis JS, Sharp TL, Laforest R et al. Tumor uptake of copper-diacetyl- bis (N(4)-methylthiosemicarbazone): effect of changes in tissue oxygenation. *J Nucl Med* 2001; 42: 655-61.
10. Lewis JS, Laforest R, Dehdashti F et al. An imaging comparison of ^{64}Cu-ATSM and ^{60}Cu-ATSM in cancer of the uterine cervix. *J Nucl Med* 2008; 49: 1177-82.
11. Yagi M, Kondo K. A ^{62}Cu-generator. *Int J Appl Radiat Isot* 1979; 30: 569-70.
12. Robinson GD Jr, Zielinski FW, Lee AW. The zinc-62/copper-62 generator: a convenient source of copper-62 for radiopharmaceuticals. *Int J Ap pl Radiat Isot* 1980; 31: 111-6.
13. Fujibayashi Y, Matsumoto K, Yonekura Y et al. A new zinc-62/copper-62 generator as a copper-62 source for PET radiopharmaceuticals. *J Nucl Med* 1989; 30:1838-42.
14. Laforest R, Dehdashti F, Lewis JS et al. Dosimetry of $^{60/61/62/64}$Cu-ATSM: a hypoxia imaging agent for PET. *Eur J Nucl Med Mol Imaging* 2005; 32: 764-70.
15. Matsumoto K, Fujibayashi Y, Yonekura Y et al. Application of the new zinc-62/copper-62 generator: an effective labeling method for ^{62}Cu-PTSM. *Int J Rad Appl Instrum B* 1992; 19: 39-44.
16. Takahashi N, Fujibayashi Y, Yonekura Y et al. Evaluation of ^{62}Cu labeled diacetyl-bis(N4-methylthiosemicarbazone) as a hypoxic tissue tracer in patients with lung cancer. *Ann Nucl Med* 2000; 14: 323-8.
17. Obata A, Kasamatsu S, McCarthy DW et al. Production of therapeutic quantities of ^{64}Cu using a 12 MeV cyclotron. *Nucl Med Biol* 2003; 30: 535-9.
18. Yoshii Y, Furukawa T, Kiyono Y et al. Copper-64-diacetyl-bis (N4-methylthiosemicarbazone) accumulates in rich regions of CD133+ highly tumorigenic cells in mouse colon carcinoma. *Nucl Med Biol* 2010; 37: 395-404.
19. Jalilian AR, Rostampour N, Rowshanfarzad P et al. Preclinical studies of [^{61}Cu]ATSM as a PET radiopharmaceutical for fibrosarcoma imaging. *Acta Pharm* 2009; 59: 45-55.
20. National electrical manufactures association performance measurements of positron emission tomographs. Rosslyn, VA: National electrical manufactures association; 2001; *NEMA standard publication NU 2*-2001:
21. DeGrado TR, Turkington TG, Williams JJ et al. Performance characteristics of a whole-body PET scanner. *J Nucl Med* 1994; 35: 1398-406.
22. Stearns CW, Fessler JA. 3D PET reconstruction with FORE and WLS-OS-EM. In: Metzler SD, Ed. *2002 IEEE Nuclear Science Symposium Conference Record*. Norfolk, VA: Institute of Electrical and Electronics Engineers, Inc.; 002, 2002; 912-5.
23. Visvikis D, Griffiths D, Costa DC et al. Clinical evaluation of 2D versus 3D whole-body PET image quality using a dedicated BGO PET scanner. *Eur J Nucl Med Mol Imaging* 2005; 32: 1050-6.
24. Bergstrom M, Martin W, Pate B. A look at anatomical and physiological brain images. *Dimens Health Serv* 1983; 60: 36.
25. Bailey DL, Meikle SR. A convolution-subtraction scatter correction method for 3D PET. *Phys Med Biol* 1994; 39: 411-24.
26. Ruangma A, Bai B, Lewis JS et al. Three-dimensional maximum a pos teriori (MAP) imaging with radiopharmaceuticals labeled with three Cu radionuclides. *Nucl Med Biol* 2006; 33: 217-26.
27. Fakhri G El, Santos PA, Badawi RD et al. Impact of acquisition geometry, image processing, and patient size on lesion detection in whole-body ^{18}F-FDG PET. *J Nucl Med* 2007; 48: 1951-60.
28. Lartizien C, Kinahan PE, Comtat C. A lesion detection observer study comparing 2-dimensional versus fully 3-dimensional whole-body PET imaging protocols. *J Nucl Med* 2004; 45: 714-23.
29. Lodge MA, Badawi RD, Gilbert R et al. Comparison of 2-dimensional and 3-dimensional acquisition for ^{18}F-FDG PET oncology studies performed on an LSO-based scanner. *J Nucl Med* 2006; 47, 23-31.
30. Chen GP, Branch KR, Alessio AM et al. Effect of reconstruction algorithms on myocardial blood flow measurement with ^{13}N-ammonia PET. *J Nucl Med* 2007; 48: 1259-65.
31. Williams HA, Robinson S, Julyan P et al. A comparison of PET imaging characteristics of various copper radioisotopes. *Eur J Nucl Med Mol Imaging* 2005; 32: 1473-80.
32. Szymański P, Frączek T, Markowicz M et al. Development of copper based drugs, radiopharmaceuticals and medical materials. *Biometals* 2012; 25:1089-112.